

## Research Article

# Implications of Changing the Asymptotic Diastolic Pressure in the Reservoir-wave Model on Wave Intensity Parameters: A Parametric Study

N. Pomella<sup>1,†</sup>, E.R. Rietzschel<sup>2</sup>, P. Segers<sup>3</sup>, Ashraf W. Khir<sup>1,\*</sup>

<sup>1</sup>Biomedical Engineering Research Theme, Brunel University London, Kingston Lane, Uxbridge, Middlesex UB8 3PH, UK

<sup>2</sup>Department of Cardiovascular Diseases, Ghent University Hospital, Ghent, Belgium

<sup>3</sup>IBiTech-bioMMeda, Ghent University, Ghent, Belgium

## ARTICLE INFO

### Article History

Received 05 March 2020

Accepted 11 May 2020

### Keywords

Variation

$P_{\infty}$

wave intensity

## ABSTRACT

Hybrid reservoir-wave models assume that the measured arterial pressure can be separated into two additive components, reservoir/windkessel and excess/wave pressure waveforms. Therefore, the effect of the reservoir volume should be excluded to properly quantify the effects of forward/backward-travelling waves on blood pressure. However, there is no consensus on the value of the asymptotic diastolic pressure decay ( $P_{\infty}$ ) which is required for the calculation of the reservoir pressure. The aim of this study was to examine the effects of varying the value of  $P_{\infty}$  on the calculation of reservoir and excess components of the measured pressure and velocity waveforms.

Common carotid pressure and flow velocity were measured using applanation tonometry and Doppler ultrasound, respectively, in 1037 healthy humans aged 35–55 years; a subset of the Asklepios population. Wave speed was determined using the PU-loop (Pressure-Velocity Loop) method, and used to separate the reservoir and wave pressures. Wave intensity analysis was performed and its parameters have been analysed with varying  $P_{\infty}$  between –75% to +75% of its initial calculated value.

The underestimation (up to –75%) of  $P_{\infty}$  (with respect to a reference value of  $48.6 \pm 21$  mmHg) did not result in any substantial change in either hemodynamic or wave intensity parameters, whereas its overestimation (from +25% to +100%) brought unrealistic increases of the studied parameters and large standard deviations. Nevertheless, reservoir pressure features and wave speed seemed insensitive to changes in  $P_{\infty}$ .

We conclude that underestimation and overestimation of  $P_{\infty}$  produce different hemodynamic effects; no change and substantially unrealistic change, respectively on wave intensity parameters. The reservoir pressure features and wave speed are independent of changes in  $P_{\infty}$ , and could be considered more reliable diagnostic indicators than other hemodynamic parameters, which are affected by changes in  $P_{\infty}$ .

© 2020 Association for Research into Arterial Structure and Physiology. Publishing services by Atlantis Press International B.V.  
This is an open access article distributed under the CC BY-NC 4.0 license (<http://creativecommons.org/licenses/by-nc/4.0/>).

## 1. INTRODUCTION

Incremental changes of arterial blood pressure are determined by forward and backward waves, originated from the heart and from the periphery, respectively. The reservoir-wave theory assumes that the measured pressure consists of two additive components: reservoir ( $P_r$ ) and “excess” pressure ( $P_{ex}$ ). This approach was successfully applied by Wang et al. [1] in canine aorta and for the calculation of venous reservoir [2]; then it was extended to any arbitrary arterial location [3,4]. Great differences of clinical and physiological hemodynamic relevant parameters, particularly the size of reflected waves, were reported in a comparison of wave speed and wave intensity analysis determined with and without the reservoir-wave approach [5].

\*Corresponding author. Email: [ashraf.khir@brunel.ac.uk](mailto:ashraf.khir@brunel.ac.uk)

<sup>†</sup>Present address: Centre for Genomics and Child Health, Blizard Institute, Queen Mary University of London, London, UK

Peer review under responsibility of the Association for Research into Arterial Structure and Physiology

Data availability statement: The data that support the findings of this study are available from the contributing author ERR.

The calculation of  $P_r$  requires fitting the diastolic decay of the measured pressure waveform to determine  $P_{\infty}$  (asymptotical value) and  $b$  (time constant) and there is no consensus over either the value of these parameters or the fitting method for their quantification. Some researchers decided not to fit  $P_{\infty}$  but kept it fixed. Specifically, Aguado-Sierra et al. [3] fixed  $P_{\infty} = 0$  mmHg for experimental data and  $P_{\infty} = 3.2$  mmHg (432.6 Pa) for computational data, following Wang et al. [2], who suggested that the asymptotical value is affected by the waterfall effect. Vermeersch et al. [6] calculated the reservoir pressure in the Asklepios population following Aguado-Sierra et al. [3]; however, they found non-physiological values of  $P_{\infty}$  with free-fitting and decided to set the asymptotical value to 0 for the entire dataset. A successive study conducted by Aguado-Sierra et al. [4] on human subjects used the same framework but imposed  $P_{\infty} = 25$  mmHg, based on previous work of Schipke et al. [7], who determined the arterial asymptotical value in anesthetized humans under fibrillation/defibrillation sequences.

In a parallel article the effects of varying fitting technique on hemodynamic and wave intensity parameters have been analysed. In this

study, we focus on the possible implications of assuming a specific value of  $P_\infty$ . It is hypothesised that different values of  $P_\infty$  would lead to different reservoir and excess waveforms, affecting hemodynamic and wave intensity parameters. By using a reference value of  $P_\infty$  and changing it by certain percentage (from  $-75\%$  to  $+100\%$ ), the comparative analysis was performed.

## 2. MATERIALS AND METHODS

### 2.1. Study Group

Details of the Asklepios Study comprising a cohort of middle-aged European participants, can be found in earlier work [8]. Briefly, the subjects were free from manifest cardiovascular disease at study initiation and were randomly sampled from the Belgian communities of Erpe-Mere and Nieuwerkerken. All examinations spanned a timeframe of 2 years and were conducted by a single observer and carried out with a single device. Clinical data, blood samples and hemodynamics measurements were acquired, as explained in the subsequent paragraphs in details.

The entire Asklepios cohort was not used for this study, but a subset of 1037 subjects. Table 1 summarizes the clinical and demographic characteristics of the study group.

### 2.2. Protocol

Subjects were asked to lay down in recumbent position, with the neck slightly hyperextended and turned approximately  $30^\circ$  contralateral during carotid scanning. Applanation tonometry and vascular echography were used to acquire blood pressure and flow velocity measurements, respectively. The measurements were not simultaneous, nonetheless acquired during the same vascular examination. The signals were post-processed and aligned using custom-made algorithms Swalen & Khir [9].

### 2.3. Pressure and Flow Measurements

A Millar pentype tonometer (SPT 301, Millar Instruments, Houston, TX, USA) was used for measuring the pressure measurements and

data were recorded at a sampling rate of 200 Hz, continuously for 20 s. Details of the applanation tonometry technique can be found in Rietzschel et al. [8] and the procedure can be summarized in two steps [10]: (a) tonometric tracings were collected from the brachial artery, divided into individual beats, using the foot of the wave as a fiducial marker, then ensemble-averaged. The averaged tracing was successively calibrated using oscillometrically measured brachial systolic and Brachial Diastolic Blood Pressure (DBP<sub>b</sub>) values as reference markers. Mean Arterial Brachial Pressure (MAP<sub>b</sub>) was calculated by numerically averaging the curve; (b) tonometry was performed on the common carotid artery, the obtained tracings were ensemble-averaged and calibrated as in step (a), assuming that diastolic and mean pressure values are fairly constant in large arteries, thus using DBP<sub>b</sub> and MAP<sub>b</sub> as reference markers. The carotid pressure waveform ( $P$ ) was scaled accordingly and used in the following analyses.

A commercially available ultrasound system (VIVID 7, GE Vingmed Ultrasound, Horten, Norway), equipped with a linear vascular transducer (12 L, 10 MHz), was used to measure blood flow velocity via Pulsed Wave Doppler, spanning 5–30 ECG-gated cardiac cycles during normal breathing. More details can be found in Rietzschel et al. [8]. The obtained DICOM images were subsequently processed [11] with home-written programs in Matlab (The MathWorks, Natick, MA, USA): maximum and minimum velocity envelopes were detected via morphological operations and averaged to obtain a velocity profile. Single velocity contours ( $U$ ) were finally obtained from this velocity profile by dividing it into individual cardiac cycles and ensemble-averaging those.

### 2.4. Data Analysis

Data analysis was performed via custom-made algorithms in Matlab.  $P$  and  $U$  waveforms were separated into their reservoir and excess components. The reservoir pressure was calculated following Aguado-Sierra et al. [3]:

$$P_r = \frac{b}{a+b} P_\infty + e^{-(a+b)t} \left[ \int_0^t aP(\vartheta) e^{(a+b)\vartheta} d\vartheta + P_0 - \frac{b}{a+b} P_\infty \right] \quad (1)$$

where  $a$ ,  $b$  and  $P_\infty$  are the systolic constant (/s) (so called because it does not appear in the diastolic equation), the diastolic constant (/s)

**Table 1** | Basic characteristics of the study group ( $n = 1037$ )

		$n$	Age (years)	Height (cm)	Weight (kg)	SBP (mmHg)	DBP (mmHg)	MAP (mmHg)	HR (bpm)
First HD	T	311	38 ± 2	171 ± 9	73 ± 13	127 ± 13	74 ± 10	96 ± 10	63 ± 9
	F	162	38 ± 2	165 ± 6	66 ± 10	123 ± 12	74 ± 10	95 ± 11	65 ± 10
	M	149	38 ± 2	178 ± 6	81 ± 11	132 ± 12	75 ± 10	98 ± 10	61 ± 8
Second HD	T	262	44 ± 2	170 ± 9	72 ± 13	129 ± 14	77 ± 10	99 ± 11	64 ± 11
	F	142	43 ± 2	165 ± 6	65 ± 10	126 ± 15	75 ± 10	97 ± 12	66 ± 10
	M	120	44 ± 1	176 ± 7	81 ± 11	133 ± 12	79 ± 10	101 ± 11	61 ± 12
Third HD	T	254	48 ± 1	170 ± 9	75 ± 14	131 ± 13	77 ± 10	100 ± 10	65 ± 9
	F	120	48 ± 1	163 ± 6	66 ± 11	128 ± 13	75 ± 9	98 ± 10	66 ± 8
	M	134	48 ± 1	175 ± 6	82 ± 11	135 ± 13	79 ± 10	102 ± 11	64 ± 11
Fourth HD	T	210	54 ± 2	168 ± 9	73 ± 13	136 ± 16	79 ± 10	104 ± 12	64 ± 10
	F	107	53 ± 2	161 ± 6	66 ± 10	136 ± 18	78 ± 11	104 ± 14	65 ± 8
	M	103	54 ± 2	175 ± 6	81 ± 11	137 ± 14	80 ± 9	104 ± 10	62 ± 12

Values are reported as mean ± SD. DBP, diastolic blood pressure; F, female; HD, half-decade; HR, heart rate; M, male; MAP, mean arterial pressure; SBP, systolic blood pressure; T, total.

and the asymptotic pressure value, respectively. In diastole (for  $T_N < t < T$ , where  $T_N$  and  $T$  are the diastolic notch time point and the duration of cardiac cycle, respectively), Equation (1) reads:

$$P_r = (\bar{P}_n - P_\infty)e^{-b(t-T_N)} + P_\infty \quad (2)$$

where  $\bar{P}_n$  is the reservoir pressure value at  $t = T_N$ .

After the calculation of diastolic  $P_r$  (which requires the determination of  $b$ ,  $\bar{P}_n$  and  $P_\infty$ ), the parameter  $a$  was calculated through the following equation:

$$P_r(T_N) = \frac{b}{a+b}P_\infty + e^{-(a+b)T_N} \left[ \int_0^{T_N} aP(\vartheta)e^{(a+b)\vartheta} d\vartheta + P_0 - \frac{b}{a+b}P_\infty \right] \quad (3)$$

The complete reservoir waveform is obtained via Equation (1) and the excess pressure from the difference:  $P_{ex} = P - P_r$ . Similar analysis held for the velocity components  $U_r$  and  $U_{ex}$ , where  $U = U_r + U_{ex}$  and  $U_r = (P - P_\infty) / \bar{R}$ , in which  $\bar{R}$  is the averaged downstream resistance defined as  $\bar{R} = (P - P_\infty) / U$ , and  $\langle P \rangle$  &  $\langle U \rangle$  are the time-averaged pressure and velocity, respectively, during diastole.

## 2.5. Fitting Algorithm Settings

The length of the fitting window was set to be the entire diastolic period and  $\bar{P}_n = P_n$ . The diastolic decay constant  $b$  was determined by fitting and bound to be non-negative, with initial condition  $b = 1/s$ , whereas  $P_\infty$  was fixed. The following seven iterations were performed for  $P_\infty$ : -25%, -50%, -75%, +25%, +50%, +75% and +100% of the reference value, detailed in Table 2 and obtained by free-fitting for each subject. The fitting algorithm was implemented using the *lsqcurvefit* function, a Matlab solver optimized for non-linear least squares problems. Relative tolerance was set at  $10^{-12}$ . The reservoir diastolic decay was calculated

via Equation (2). For the determination of the systolic time constant  $a$ , the same Matlab function (*lsqcurvefit*) was used to solve Equation (3), with initial condition  $a = 10/s$  [3].

The following hemodynamic parameters were calculated: the maxima of  $P_r$  and  $P_{ex}$  ( $P_r$  max and  $P_{ex}$  max, respectively), the time integral of reservoir pressure (PRI) and integral of excess pressure (PEI) curves, respectively (therefore having units of Pa·s) and the maxima of  $U_r$  and  $U_{ex}$  ( $U_r$  max and  $U_{ex}$  max, respectively).

Examples of varying waveforms (reservoir and excess, pressure and velocity) with  $P_\infty$  are shown in Figure 1, with artificially extended reservoir pressure contours displayed in Figure 2 (where the ratios among  $P_\infty$  values are clearer).

## 2.6. Wave Intensity Analysis

Wave intensity analysis was performed on excess waveforms ( $P_{ex}$ ,  $U_{ex}$ ) for each subject. Assuming that reflected waves were absent during the early systolic portion of each cardiac cycle [12], the slope

**Table 2** | Actual asymptotical pressure values used in the analysis ( $n = 1037$ ).

$P_\infty$ variation (w.r.t.R)	$P_\infty$ value (mmHg)
-75%	12.2 ± 5.3
-50%	24.4 ± 10.5
-25%	36.4 ± 15.7
0% (R)	48.6 ± 21.0
+25%	60.8 ± 26.2
+50%	72.9 ± 31.4
+75%	85.0 ± 36.6
+100%	97.2 ± 41.8

Values are reported as mean ± SD. w.r.t.R, with respect to the reference value (R).

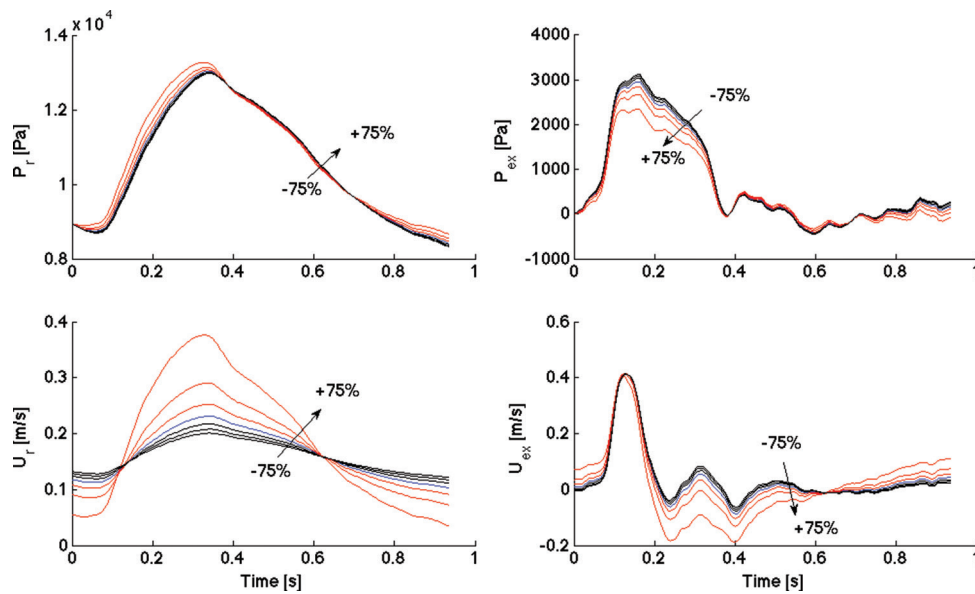


**Figure 1** | Comparisons of reservoir pressure waveforms ( $P_r$ , Top left), excess pressure waveforms ( $P_{ex}$ , Top right), reservoir velocity waveforms ( $U_r$ , Bottom left) and excess velocity waveforms ( $U_{ex}$ , Bottom right) for one subject, among positive (up to +75%) and negative (up to -75%) variations of  $P_\infty$ , with respect to the reference value (R). The +100% variation is not reported because it would alter the scale. An arrow indicates the direction of increasing variation, from negative to positive.

of the linear part of the  $P_{ex}U_{ex}$  loop was used to calculate the corresponding wave speed value (m/s) using the following equation:

$$c = \frac{1}{\rho} \frac{\Delta P_{\pm}}{\Delta U_{\pm}} \quad (4)$$

where the relationship between  $P$  and  $U$  over the early systolic part of the loop is linear (Figure 3). Blood density  $\rho$  was assumed equal to 1050 kg/m<sup>3</sup>. Then, the wave intensity  $dI = dPdU$  (W/m<sup>2</sup>) was separated into its forward- and backward-travelling components [13]:

$$dI_{\pm} = dP_{\pm}dU_{\pm} = \pm \frac{1}{4\rho c} (dP \pm \rho c dU)^2 \quad (5)$$

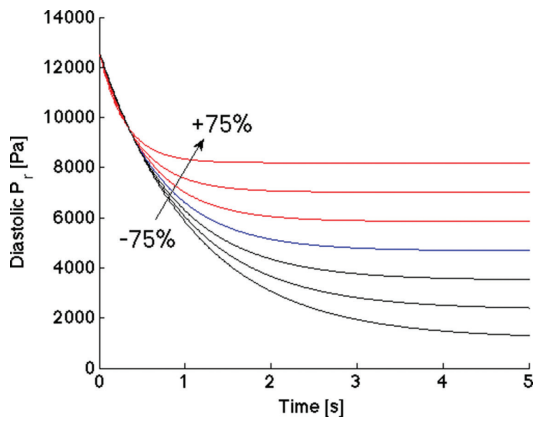


**Figure 2** | Comparison of diastolic reservoir pressure decay among positive (up to +75%) and negative (up to -75%) variations of  $P_{\infty}$ , with respect to the reference value (R) for one subject and artificially extended compared to Figure 1. An arrow indicates the direction of increasing variation, from negative to positive.

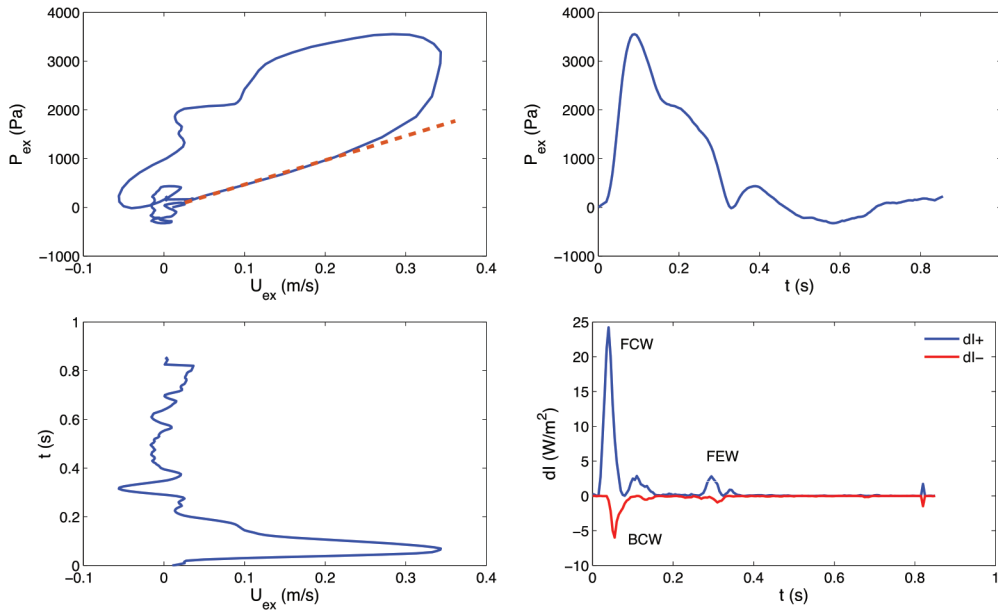


**Figure 3** | Example of  $P_{ex}U_{ex}$  loop (Top left),  $P_{ex}$  contour (Top right),  $U_{ex}$  contour (Bottom left) and corresponding wave intensity [Bottom left; see Equation (5)] for one subject. A straight line highlighting the slope of the linear portion is superimposed on the  $P_{ex}U_{ex}$  loop [see Equation (4)]. Forward Compression Wave (FCW), Backward Compression Wave (BCW) and Forward Expansion Wave (FEW) are labelled in the wave intensity plot.  $dI_{+}$ , forward wave intensity component;  $dI_{-}$ , backward wave intensity component.

After the calculation of wave speed and wave intensity, relevant wave intensity parameters were extracted. The area (J/m<sup>2</sup>) of the Forward Compression Wave (FCW), generated by the contraction of the left ventricle, was calculated from the area of the early-systolic peak observed in  $dI_{+}$  (Figure 3). Similarly, the area of the Backward Compression Wave (BCW), which is attributed to reflections from the head microcirculation if it is measured in the common carotid artery, was determined from the area, of the mid-systolic peak present in  $dI_{-}$ . Finally, the area of the Forward Expansion Wave (FEW), which is generated by the decrease in shortening velocity of the left ventricle in late systole, was determined from the area of the late-systolic peak seen in  $dI_{+}$ .

### 2.7. Statistical Analysis

All values are reported as mean  $\pm$  SD, relative to the whole cohort, in the text, tables and figures. SPSS Statistics (version 20, IBM, Armonk, NY, USA) was used to design the statistical analysis. Hemodynamic and wave intensity parameters were compared via one-way analysis of variance followed by Tukey’s *post-hoc*. Significance threshold was set at adjusted  $p = 0.05$ .

### 3. RESULTS

All changes are referred to the reference value for that particular parameter (as detailed in Table 2).

$P_{ex}$  max (Figure 4) did not significantly change with negative  $P_{\infty}$  variations (-25%, -50%, -75%) but decreased significantly with respect to the reference value (w.r.t.R) with positive  $P_{\infty}$  variations, up to +50%; then it increased again. The biggest change w.r.t.R was at +50% variation and its amplitude was -12% ( $p < 0.05$ ). SD did not substantially change with  $P_{\infty}$  variations.

$P_r$  max (Figure 4) did not significantly change: it had a tendency to decrease w.r.t.R with negative  $P_\infty$  variations and to increase with positive  $P_\infty$  variations, up to +50%. The maximum change w.r.t.R was recorded at +50% and its amplitude was +1.6% ( $p > 0.05$ ). SD did not substantially change with  $P_\infty$  variations.

PEI (Figure 4) decreased (significantly w.r.t.R) with positive  $P_\infty$  variations and slightly increased (significantly w.r.t.R, except at -75%) with negative  $P_\infty$  variations. The biggest changes w.r.t.R were: -26% ( $p < 0.05$ ) at the biggest positive variation (+100%) and +5% ( $p < 0.05$ ) at the opposite side (-75% variation). PRI (Figure 4) had a tendency to decrease with negative  $P_\infty$  variations and to increase with positive variations. Overall, its value did not substantially change: the maximum increase was at +100% variation and its corresponding amplitude was +3% ( $p < 0.05$ ). SD did not substantially change for both PEI and PRI.

$U_r$  max and  $U_{ex}$  max (Figure 4) had very high SD at positive  $P_\infty$  variations.  $U_r$  max did not significantly change w.r.t.R with negative  $P_\infty$  variations but had a tendency to decrease (maximum change: -14% at -75% variation) whereas it significantly increased w.r.t.R with positive  $P_\infty$  variations (maximum change: +100% at +50% variation). At +75% and +100% iterations, it had a tendency to decrease again. The same behaviour applied to  $U_{ex}$  max: the maximum changes had amplitudes of +106% at +50% variation and -3% at -75% variation, respectively. The increases in the positive direction were significant whereas all decreases in the negative direction were non-significant.

The diastolic constant  $b$  (Figure 5) did not change significantly w.r.t.R, with all negative  $P_\infty$  variations, but had a tendency to decrease, whereas it increased (significantly w.r.t.R) with positive  $P_\infty$  variations, up to +75%. The SD substantially increased with

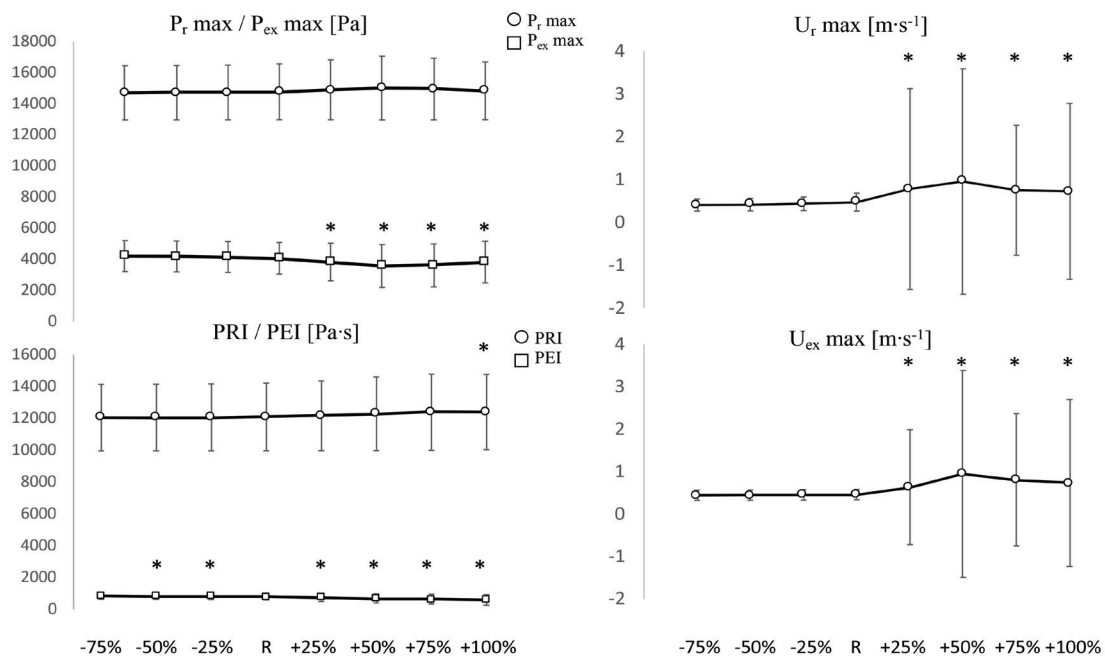


**Figure 4** | Comparisons of  $P_r$  max and  $P_{ex}$  max (Top left),  $U_r$  max (Top right), PRI and PEI (Bottom left) and  $U_{ex}$  max (Bottom right) values among positive (+25%, +50%, +75%, +100%) and negative (-25%, -50%, -75%) variations of  $P_\infty$ , with respect to the reference value (R). \*Significant difference with respect to R ( $p < 0.05$ ). Y-axis units are reported in each figure title. Values are reported as mean  $\pm$  SD ( $n = 1037$ ).

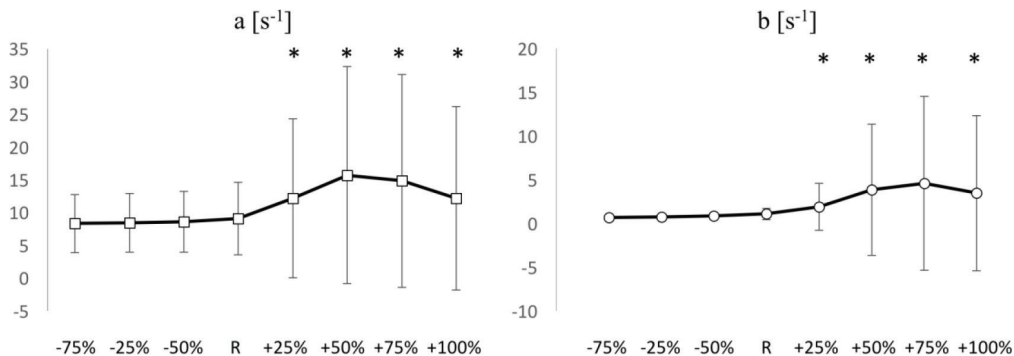


**Figure 5** | Comparisons of rate constant  $a$  (Left) and diastolic rate constant  $b$  (Right), among positive (+25%, +50%, +75%, +100%) and negative (-25%, -50%, -75%) variations of  $P_\infty$ , with respect to the reference value (R). \*Significant difference with respect to R ( $p < 0.05$ ). Y-axis units are reported in each figure title. Values are reported as mean  $\pm$  SD ( $n = 1037$ ).

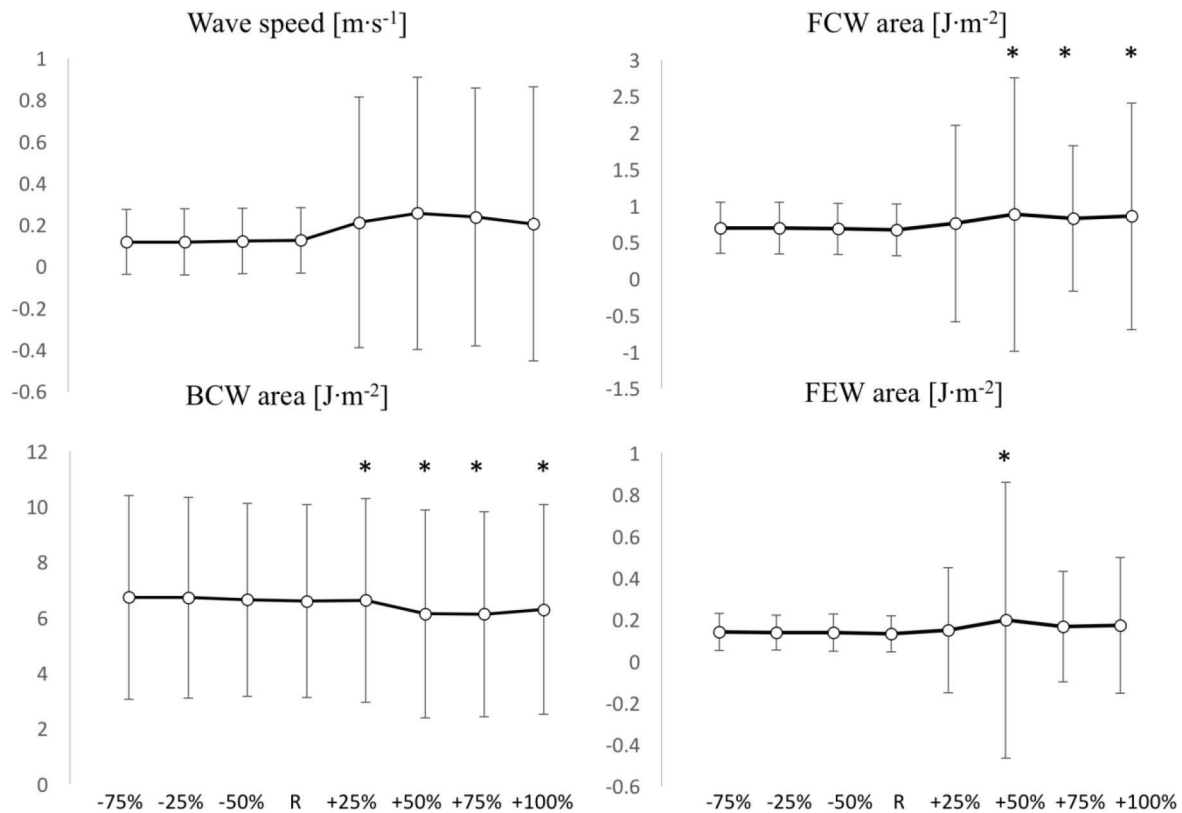


**Figure 6** | Comparisons of wave speed  $c$  (Top left), FCW area (Top right), BCW area (Bottom left) and FEW area (Bottom right) values among positive (+25%, +50%, +75%, +100%) and negative (−25%, −50%, −75%) variations of  $P_{\infty}$ , with respect to the reference value (R). \*Significant difference with respect to R ( $p < 0.05$ ). Y-axis units are reported in each figure title. Values are reported as mean  $\pm$  SD ( $n = 1037$ ).

positive variations. The systolic constant  $a$  (Figure 5) had also a tendency to decrease (non-significantly w.r.t.R) with negative  $P_{\infty}$  variations whereas significantly increased with all positive  $P_{\infty}$  variations, up to +50%, resembling the behaviour of  $b$ .

Wave speed (Figure 6) did not substantially change: it slightly increased (non-significantly w.r.t.R) with negative  $P_{\infty}$  variations (maximum change: +2% at −75% iteration) and tended to decrease (non-significantly w.r.t.R) with positive  $P_{\infty}$  variations (maximum change: −7% at +75% iteration). SD tended to remain stable.

In the context of wave intensity analysis, FCW area (Figure 6) increased with positive variations (significantly w.r.t.R, except for +25% iteration) whereas it remained unchanged with negative variations. Maximum changes were +32% at +50% variation in the positive direction and +4% ( $p > 0.05$ ) at −75% variation in the negative direction. FEW area (Figure 6) had a tendency to increase in both directions of variation, although its increases were all non-significant, except for the +50% iteration. Maximum changes were +49% at +50% variation in the positive direction and +7% at −75% variation in the negative direction. SD tended to increase in the positive direction and to remain stable in the negative direction, for both FCW and FEW areas.

Finally, BCW area (Figure 6) significantly increased in the positive direction and non-significantly changed in the negative direction. The maximum changes were: −7% ( $p > 0.05$ ) at −75% variation and +103% at +50% variation.

## 4. DISCUSSION

The concept of reservoir pressure has already been used in research and clinical studies, we believe it is crucially important to establish the effect of the value of  $P_{\infty}$  on the determination of wave speed and wave intensity analysis, which are being used to characterise arterial stiffness and cardio-arterial interaction, respectively. We determined  $P_{\infty}$  by fitting the diastolic pressure decay as described earlier [3], calculated wave speed using the PU-loop (Pressure-Velocity Loop) [12] and carried out wave intensity analysis [13]. We varied the value of  $P_{\infty}$  from −75% to +100% and calculated the corresponding values of hemodynamic parameters.

The concerns pertaining the validity of the reservoir-wave approach continues [14,15] and the suitability of the technique is hotly debated both in the research and clinical fields [16–18]. However, the scope of this parametric study was to assess the sensitivity of the derived parameters as a function of the value of the asymptotic pressure. Further, the suitability of using a single exponential function to model the diastolic decay is also questioned by the recent work of Parker [15], who suggested that multi-exponential models might be more appropriate to describe the pressure waveform in diastole, reflecting the behaviour of many high-order modes of the waves. In this study, however, we chose to model the pressure decay with a single exponential and a single asymptotic value to allow direct comparisons with previous work.

The analysis in the present study was performed on clinical vascular data of a middle aged healthy human cohort. Hemodynamic and wave intensity parameters were compared using different  $P_{\infty}$  values in the fitting of the reservoir pressure and velocity waveforms, assuming the reservoir-wave hypothesis for the decomposition of the measured arterial pressure.

Wave intensity analysis requires value of wave speed for the determination of the forward and backward wave intensities. Wave speed in this study was determined using the PU-loop method [Equation (4)], which assumes the absence of reflected waves during the early part of systole, and that waves are unidirectional. Although Segers et al. [19] questioned this assumption regarding the loop techniques and found that PU-loop method may lead to an overestimation of wave speed in the carotid artery, Borlotti et al. [11] and Pomella et al. [20,21] have successfully used the lnDU-loop (Diameter-Velocity loop) technique also in the carotid artery with the later studies carried out during exercise. While we acknowledge the possible existence of reflected waves in the carotid artery in early systole, we do not consider this to be relevant to the scope of this study and should not impact the results or the conclusions related to the reservoir-wave approach.

Table 2 reports the actual  $P_{\infty}$  values used in this analysis. It emerged that asymptotical pressure values smaller than the used reference ( $48.6 \pm 21.0$  mmHg) did not bring substantial changes to hemodynamic and wave intensity parameters, whereas greater values brought significant “unrealistic” changes to almost all hemodynamic and wave intensity parameters, as demonstrated by the high standard deviations involved. However, these unrealistic changes were not observed in the reservoir pressure features, such as  $P_r$ , max and PRI. Overestimation of  $P_{\infty}$  did not induce unrealistic values of wave speed either. Hence, reservoir pressure and wave speed, being substantially independent of the fitting parameter, could be used as reliable diagnostic indicators.

It is also important to emphasize that the reference value of  $P_{\infty}$  is inevitably cohort-dependent, but considering the width of the range of pressure values for which significant changes in the analysed physiological features could not be seen, we can confidently state that  $12.2 < P_{\infty} < 48.6$  mmHg would be a safe range to work with. This is in line with results of Hughes et al. [22], who performed a meta-analysis of asymptotic and mean circulatory filling pressure values in humans and other mammals, for which cessation of blood flow was involved, and found a mean  $P_{\infty}$  value of 26.5 mmHg.

#### 4.1. Limitations

Pressure and velocity measurements were not taken simultaneously, but sequentially, as explained in the Methods section. However, the time interval between the pressure and velocity recordings was short [11], and rapid physiological perturbations were not involved in this study. Therefore, it can be safely assumed that the hemodynamic parameters did not change significantly between recordings and the sequential recordings of the data did not impact the analysis, results or conclusions negatively.

## 5. CONCLUSION

It is vitally important to use the correct analysis of the reservoir pressure to obtain an accurate value of the asymptotic diastolic

pressure decay ( $P_{\infty}$ ). Underestimation of  $P_{\infty}$  (up to  $-75\%$ ) w.r.t.R does not result in substantial changes to the hemodynamic and wave intensity parameters. Oppositely, overestimation (greater than  $+25\%$ ) of  $P_{\infty}$  resulted in unrealistic increases of the studied parameters and induced large standard deviations.

The reservoir pressure and wave speed determined in this study are insensitive to a wide range of  $-75\%$  to  $+100\%$  changes of  $P_{\infty}$ . As such, the reservoir pressure and wave speed are independent of changes to  $P_{\infty}$  and could be more reliable diagnostic indicators compared to other parameters that are sensitive to changes in  $P_{\infty}$  such as wave intensity analysis parameters.

## CONFLICTS OF INTEREST

The authors declare they have no conflicts of interest.

## AUTHORS' CONTRIBUTION

AWK study concept and design. NP formal data analysis. EER data acquisition. NP and AWK manuscript drafting and development. AWK and PS data interpretation and manuscript editing. NP, EER, PS and AWK proofreading and editing final draft.

## FUNDING

Fund for Scientific Research Flanders - FWO G.0427.03.

## REFERENCES

- [1] Wang JJ, O'Brien AB, Shrive NG, Parker KH, Tyberg JV. Time-domain representation of ventricular-arterial coupling as a windkessel and wave system. *Am J Physiol Heart Circ Physiol* 2003;284:H1358–H68.
- [2] Wang JJ, Flewitt JA, Shrive NG, Parker KH, Tyberg JV. Systemic venous circulation. Waves propagating on a windkessel: relation of arterial and venous windkessels to systemic vascular resistance. *Am J Physiol Heart Circ Physiol* 2006;290:H154–H62.
- [3] Aguado-Sierra J, Alastruey J, Wang JJ, Hadjiloizou N, Davies J, Parker KH. Separation of the reservoir and wave pressure and velocity from measurements at an arbitrary location in arteries. *Proc Inst Mech Eng H* 2008;222:403–16.
- [4] Aguado-Sierra J, Davies JE, Hadjiloizou N, Francis D, Mayet J, Hughes AD, et al. Reservoir-wave separation and wave intensity analysis applied to carotid arteries: a hybrid 1D model to understand haemodynamics. *Conf Proc IEEE Eng Med Biol Soc* 2008;2008:1381–4.
- [5] Borlotti A, Park C, Parker KH, Khir AW. Reservoir and reservoir-less pressure effects on arterial waves in the canine aorta. *J Hypertens* 2015;33:564–74.
- [6] Vermeersch SJ, Rietzschel ER, De Buyzere ML, Van Bortel LM, Gillebert TC, Verdonck PR, et al. The reservoir pressure concept: the 3-element windkessel model revisited? Application to the Asklepios population study. *J Eng Math* 2009;64:417–28.
- [7] Schipke JD, Heusch G, Sani AP, Gams E, Winter J. Static filling pressure in patients during induced ventricular fibrillation. *Am J Physiol Heart Circ Physiol* 2003;285:H2510–H15.

- [8] Rietzschel ER, De Buyzere ML, Bekaert S, Segers P, De Bacquer D, Cooman L, et al. Rationale, design, methods and baseline characteristics of the Asklepios Study. *Eur J Cardiovasc Prev Rehabil* 2007;14:179–91.
- [9] Swalen MJP, Khir AW. Resolving the time lag between pressure and flow for the determination of local wave speed in elastic tubes and arteries. *J Biomech* 2009;42:1574–7.
- [10] Segers P, Rietzschel ER, De Buyzere ML, Vermeersch SJ, De Bacquer D, Van Bortel LM, et al. Noninvasive (input) impedance, pulse wave velocity, and wave reflection in healthy middle-aged men and women. *Hypertension* 2007;49:1248–55.
- [11] Borlotti A, Khir AW, Rietzschel ER, De Buyzere ML, Vermeersch S, Segers P. Noninvasive determination of local pulse wave velocity and wave intensity: changes with age and gender in the carotid and femoral arteries of healthy human. *J Appl Physiol* (1985) 2012;113:727–35.
- [12] Khir AW, O'Brien A, Gibbs JSR, Parker KH. Determination of wave speed and wave separation in the arteries. *J Biomech* 2001;34:1145–55.
- [13] Parker KH, Jones CJH. Forward and backward running waves in the arteries: analysis using the method of characteristics. *J Biomech Eng* 1990;112:322–6.
- [14] Westerhof N, Segers P, Westerhof BE. Wave separation, wave intensity, the reservoir-wave concept, and the instantaneous wave-free ratio: presumptions and principles. *Hypertension* 2015;66:93–8.
- [15] Parker KH. The reservoir-wave model. *Artery Res* 2017;18:87–101.
- [16] Davies JE, Lacy P, Tillin T, Collier D, Cruickshank JK, Francis DP, et al. Excess pressure integral predicts cardiovascular events independent of other risk factors in the conduit artery functional evaluation substudy of Anglo-Scandinavian cardiac outcomes trial. *Hypertension* 2014;64:60–8.
- [17] Westerhof N, Westerhof B, Segers P. Application of the wave-reservoir approach to different aortic sites: overstretching the concept. *J Hypertens* 2018;36:963–4.
- [18] Armstrong MK, Schultz MG, Picone DS, Black JA, Dwyer N, Roberts-Thomson P, et al. Associations of reservoir-excess pressure parameters derived from central and peripheral arteries with kidney function. *Am J Hypertens* 2020;33: 325–30.
- [19] Segers P, Swillens A, Taelman L, Vierendeels J. Wave reflection leads to over- and underestimation of local wave speed by the PU- and QA-loop methods: theoretical basis and solution to the problem. *Physiol Meas* 2014;35:847–61.
- [20] Pomella N, Wilhelm EN, Kolyva C, González-Alonso J, Rakobowchuk M, Khir AW. Common carotid artery diameter, blood flow velocity and wave intensity responses at rest and during exercise in young healthy humans: a reproducibility study. *Ultrasound Med Biol* 2017;43:943–57.
- [21] Pomella N, Wilhelm EN, Kolyva C, González-Alonso J, Rakobowchuk M, Khir AW. Noninvasive assessment of the common carotid artery hemodynamics with increasing exercise work rate using wave intensity analysis. *Am J Physiol Heart Circ Physiol* 2018;315:H233–H41.
- [22] Hughes AD, Parker K, Khir A. Zero flow pressure (P<sub>infinite</sub>) is larger than mean circulatory filling pressure. A systematic review and meta-analysis. *Artery Res* 2018;24:94.